ARTICLE

Materials chemistry of triplet dynamic nuclear polarization

Koki Nishimura,[a] Hironori Kouno,[a] Yusuke Kawashima,[a] Kana Orihashi,[a] Saiya Fujiwara,[a] Kenichiro Tateishi,[b] Tomohiro Uesaka,[b] Nobuo Kimizuka[a] and Nobuhiro Yanai*,[a,c]

Dynamic nuclear polarization with photo-excited triplet electrons (triplet-DNP) has the potential to enhance the sensitivity of nuclear magnetic resonance (NMR) and magnetic resonance imaging (MRI) at a moderate temperature. While much efforts have been devoted to obtaining the large nuclear polarization based on triplet-DNP, the application of triplet-DNP has been limited to nuclear physics experiments. The recent introduction of materials chemistry into the field of triplet-DNP realizes the air-stable and water-soluble polarizing agents as well as the hyperpolarization of nanomaterials with a large surface area such as nanoporous metal-organic frameworks (MOFs) and nanocrystal dispersion in water. This Feature Article overviews the recently-emerged materials chemistry of triplet-DNP that paves new paths towards unprecedented biological and medical applications.

1. Introduction

Nuclear magnetic resonance (NMR) spectroscopy and magnetic resonance imaging (MRI) are powerful analysis techniques and applied in various fields in physics, chemistry, biology, and medicine.[1-5] NMR measurements provide rich information such as chemical structures, molecular dynamics, and morphologies. MRI is indispensable in modern medical diagnosis. However, the biggest disadvantage of NMR and MRI is their poor sensitivity that requires a high concentration of analytes and a long integration time. The sensitivity of NMR depends on the polarization P defined as follows,

$$P = \frac{N_\alpha - N_\beta}{N_\alpha + N_\beta} = \tanh\left(\frac{\gamma \hbar B_0}{2kT}\right) \tag{1}$$

where N_α and N_β are the number of spins in the α and β state, respectively, γ is the gyromagnetic ratio of nucleus or electron, $\hbar$ is the Plank constant, B_0 is the strength of the external magnetic field, k is the Boltzmann constant, and T is the temperature. The energy gap of nuclear spins between the nuclear α and β states is generally lower than 5 µeV at the ambient condition, which means the spin polarization of less than 0.01%.

One of the simplest ways to improve the sensitivity of NMR is increasing the static magnetic field (B_0), but it already reached nearly the upper limit using the superconducting techniques, and the instrumental cost with the giant magnets limits the accessibility.[6, 7] To overcome this situation, various

techniques to make a biased non-equilibrium nuclear spin state, so-called hyperpolarization, have been developed such as spin-exchange optical pumping (SEOP),[8-11] parahydrogen induced hyperpolarization (PHIP),[12-16] signal amplification by reversible exchange (SABRE)[17-20] and dynamic nuclear polarization (DNP).[21-32] In SEOP, the electron spin polarization in alkali metals, produced via the spin-selective excitation by circularly polarised light, is utilized to hyperpolarize noble gases (^{3}He and ^{129}Xe) for making MRI contrast agents.[33-36] PHIP and SABRE transfer the polarization of parahydrogen to ^{1}H or ^{13}C spins of target molecules by a hydrogenation reaction or a temporary complexation.[37-40] Details of these techniques are well-documented in recent reviews.[41-46]

DNP is based on the polarization transfer from electron spins to nuclear spins. Due to the larger gyromagnetic ratio of an electron than those of nuclei, the thermal-equilibrium polarization of electron spins is ca. 660 and 2600 times larger than those of ^{1}H and ^{13}C spins, respectively, at room temperature. At cryogenic condition (< 4K), the electron spin polarization reaches 100% (equation 1). Ardenkjær-Larsen et al. invented the dissolution-DNP (d-DNP) technique where the highly sensitive NMR spectroscopy can be achieved by the polarization transfer from electron spins of paramagnetic radicals to nuclear spins of target compounds below 4K, followed by the quick dissolution of the frozen sample and transfer to an NMR spectrometer.[21] This d-DNP method has successfully hyperpolarized a variety of biology-relevant compounds and come on the stage of the clinical trial of cancer imaging.[47-52] On the other hand, the use of cryogenic conditions remains a grand challenge of d-DNP, which inevitably increases the instrumental cost and limits the direct hyperpolarization in living systems. There is another DNP method using permanent paramagnetic species in solution, known as Overhauser-DNP.[53-57] While it allows the hyperpolarization of various substances in solution, the polarization enhancement is theoretically limited

a. Department of Chemistry and Biochemistry, Graduate School of Engineering, Center for Molecular Systems (CMS), Kyushu University, 744 Moto-oka, Nishi-ku, Fukuoka 819-0395, Japan.
E-mail: yanai@mail.cstm.kyushu-u.ac.jp
b. Cluster for Pioneering Research, RIKEN, RIKEN Nishina Center for Accelerator-Based Science, 2-1 Hirosawa, Wako, Saitama 351-0198, Japan.
c. PRESTO, JST, Honcho 4-1-8, Kawaguchi, Saitama 332-0012, Japan.

to 660 times for ^1H spins at the thermal equilibrium (equation 1).

To overcome these challenges of DNP, the use of non-equilibrium polarization of electron spins can be promising for the room-temperature hyperpolarization.[58-60] One of the methods based on this concept is DNP using photo-excited triplet electrons as a polarization source (triplet-DNP, Fig. 1).[61-80] The triplet state has three degenerated sublevels, and the degeneracy is removed by zero-field and Zeeman splitting. Polarized triplet electrons are generated by a population of a specific sublevel via spin-selective intersystem crossing (ISC). Then, the high polarization of triplet electron spins is transferred to nuclear spins by integrated solid effect (ISE) with microwave irradiation under a magnetic field sweep. Thanks to the temperature-insensitive non-equilibrium polarization of photo-excited triplets,[79, 81] it is possible to achieve a high polarization even at room temperature. Wenckebach and coworkers reported the first room-temperature triplet-DNP

with a large ^1H signal enhancement of 5500.[61] After optimizing experimental and sample conditions, Tateishi et al. achieved a significantly high ^1H spin polarization of 34% with an enhancement of 250,000 at room temperature.[79]

Despite its great potential, the application of triplet-DNP has been limited to the nuclear physics experiments such as polarized targets. The triplet-DNP process has been developed and optimized in the field of physics,[82-88] in which the matrix has been limited to the dense solids of aromatic compounds, and pentacene has been the only option of the polarizing agent. [61-80, 84] We propose that the introduction of materials chemistry to triplet-DNP makes it applicable to biology and medical fields (Fig. 2). By increasing the surface area of the polarization matrices such as nanoporous materials and nanoparticles, there would be more chances to transfer the nuclear polarization to target biology-relevant molecules. The development of non-pentacene polarizing agents with high air-stability and water solubility would allow the direct doping of polarizing agents into water and other biological substances.

In this Feature Article, we start with a summary of the history and mechanism of triplet-DNP and then discuss the recent advancements and prospects of triplet-DNP from the viewpoint of materials chemistry.

2. Background of triplet-DNP

Brief history of triplet-DNP

The polarization transfer from photo-excited triplet electron spins to nuclear spins was first reported by Hausser et al. in an anthracene single crystal.[89] In the following early days, the polarization transfer was observed without using microwave by applying a magnetic field in the anti-level crossing region or by relaxation during triplet exciton diffusion.[90-94] The microwave-induced polarization transfer from photo-excited triplet electron spins to nuclear spins was demonstrated by Deimling
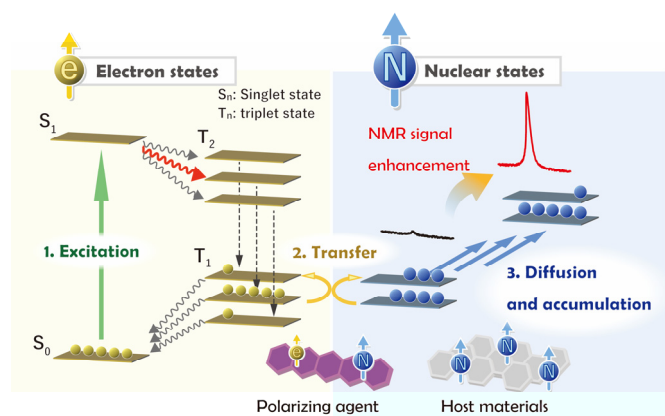
Fig. 1 Typical scheme of triplet-DNP. Photoexcitation of the polarizing agent is followed by spin-selective intersystem crossing (ISC). The resulting large electron spin polarization is transferred to the nuclear spin polarization through the integrated solid effect (ISE).
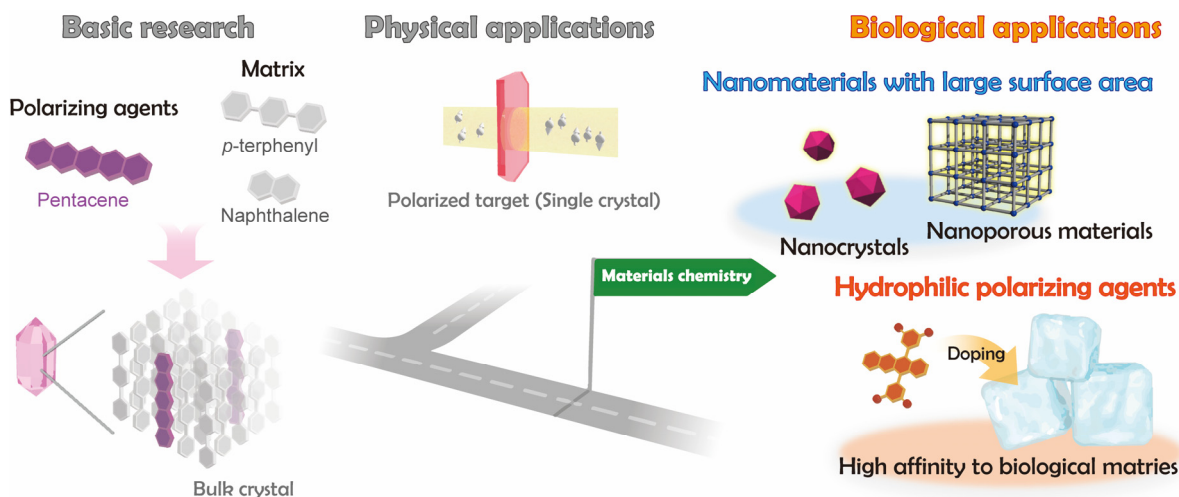
Fig. 2 Schematic representation of basic concept of this Feature Article. The basic physics of triplet-DNP has been developed and applied to nuclear physics experiments. The introduction of materials chemistry to triplet-DNP would make triplet-DNP more accessible by employing nanoporous materials and nanocrystals and more feasible by developing air-stable and water-soluble polarizing agents, paving a way towards biological applications.

et al. for the first time, but the enhancement factor was quite small (10).[95] In 1990, Wenckebach and coworkers developed the more efficient polarization transfer method with concomitant application of microwave irradiation and magnetic field sweep (ISE) to achieve the 5,000-fold enhancement of ^{1}H polarization, which was the first demonstration of ^{1}H polarization enhancement beyond the theoretical limit of 660 with paramagnetic radicals.[61] After that, the enhancement factor was further increased by several groups' efforts to optimize the experimental and sample conditions.[63-73] Finally, the ^{1}H polarization reached 80% at 25 K in a pentacene-doped naphthalene single crystal[88] and 34% at room temperature in a pentacene-doped p-terphenyl-d_4 single crystal.[79] The deuteration of pentacene and matrix molecules helps to increase the polarization enhancement by suppressing the nuclear spin-lattice relaxation. The highly polarized single crystals were used as polarized target.[82-88]

While the polarization enhancement based on triplet-DNP has successfully reached the level of practical applications, it requires the precise alignment of a single crystal, and biology-relevant molecules cannot be accommodated in the single crystal. Based on these fundamental developments of triplet-DNP in physics, it's the turn of chemistry to make it useful in biological applications.

Energy level and population of triplet sublevels

The basic principles and methods of triplet-DNP are nicely summarized in a book written by Takeda.[96] We extract the minimum components here for the sake of readers by taking the pentacene-doped p-terphenyl crystal as an example.

The triplet state has three sublevels, and the different population among these sublevels can be used as the polarization source. In the absence of a magnetic field, the energy levels of the three sublevels are determined by the zero-field splitting (ZFS) interaction ($\mathcal{H}_{\mathrm{ZFS}}$) that originates from dipole-dipole interaction between the two electron spins in the triplet state. ZFS Hamiltonian $\mathcal{H}_{\mathrm{ZFS}}$ is written by using a spin operator $\boldsymbol{S}$ ($S = 1$) as

$$\mathcal{H}_{\mathrm{ZFS}} = D\left[S_Z^2 - \frac{1}{3}S(S+1)\right] + E(S_X^2 - S_Y^2) \qquad (2)$$

where D and E are ZFS parameters. In the absence of the external field, ZFS Hamiltonian is diagonalized in a basis set $\{|X\rangle, |Y\rangle, |Z\rangle\}$ defined as

$$|X\rangle = \frac{1}{\sqrt{2}}(|-1\rangle - |+1\rangle), \qquad (3\text{-}1)$$

$$|Y\rangle = \frac{i}{\sqrt{2}}(|-1\rangle + |+1\rangle), \qquad (3\text{-}2)$$

$$|Z\rangle = |0\rangle, \qquad (3\text{-}3)$$

where $\{|+1\rangle, |0\rangle, |-1\rangle\}$ are the eigenstates of S_Z. In the course of the transition from the S_1 state to the T_n state by ISC, the spin-orbit coupling selectively populates a specific triplet sublevel. For the benchmark polarizing agent pentacene, the populations over the triplet substates $|X\rangle$, $|Y\rangle$, and $|Z\rangle$ are reported to be 0.76, 0.16, and 0.08, respectively.[62, 81, 98]

Under an external magnetic field, the triplet energy levels are further affected by the Zeeman interaction ($\mathcal{H}_Z$), and the total Hamiltonian is given by

$$\mathcal{H} = \mathcal{H}_{\mathrm{ZFS}} + \mathcal{H}_Z,$$

$$\mathcal{H}_Z = \omega_0 S_Z, \qquad (4)$$

where ω_0 is electron resonance frequency. Using the $\{|X\rangle, |Y\rangle, |Z\rangle\}$ basis set, the total Hamiltonian can be expressed in a matrix form as

$$\mathcal{H} = \begin{pmatrix} X & -i\omega_0\cos\Theta & i\omega_0\sin\Theta\sin\Phi \\ i\omega_0\cos\Theta & Y & -i\omega_0\sin\Theta\cos\Phi \\ -i\omega_0\sin\Theta\sin\Phi & i\omega_0\sin\Theta\cos\Phi & Z \end{pmatrix},$$

$$(5)$$

where Θ and Φ represent the orientation of the external field with respect to the principal axis system of the ZFS tensor (Fig. 3a). The energy levels of triplet state $\{E_{-1}, E_0, E_{+1}\}$ are obtained as eigenvalues of this Hamiltonian. When the
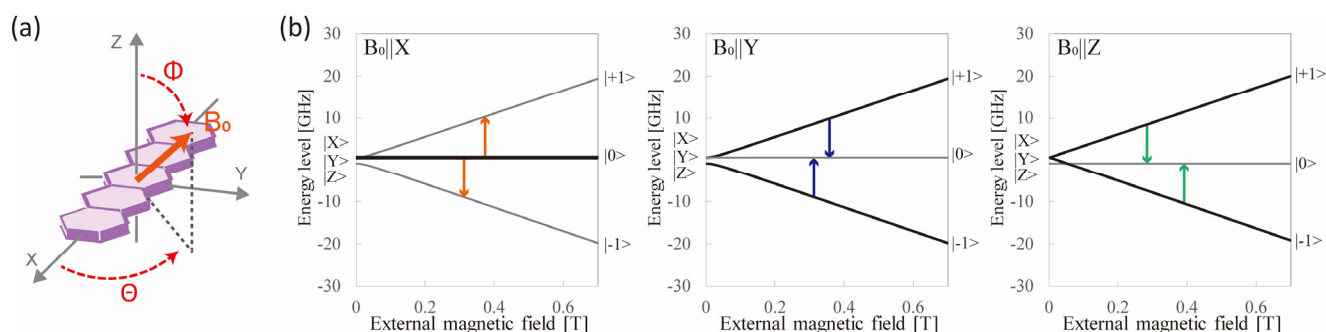
Fig. 3 (a) Principal axes of the ZFS interaction of the photo-excited pentacene triplet. The standard convention for assigning the labels X, Y and Z to the molecular axes is such that $|Z\rangle$ is the level with the largest separation from the center of gravity, $|X\rangle$ with the second largest separation, and $|Y\rangle$ is in the middle.[97] (b) Triplet energy levels of pentacene when $\mathbf{B_0}||\mathbf{X}$ (left), $\mathbf{B_0}||\mathbf{Y}$ (centre), and $\mathbf{B_0}||\mathbf{Z}$ (right). The arrows show the transitions of absorption and emission induced by X-band (~9 GHz) microwave irradiation.
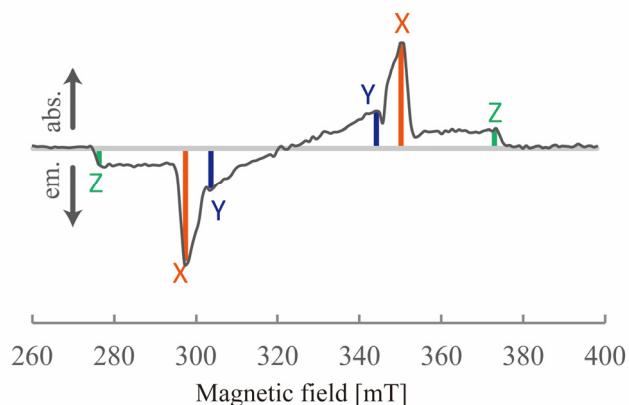
Fig. 4 EPR spectrum of photo-excited pentacene doped in *p*-terphenyl crystalline powder. The absorption and emission peaks originating from specifically-oriented pentacene molecules are marked by solid lines ($\mathbf{B_0}||\mathbf{X}$: orange, $\mathbf{B_0}||\mathbf{Y}$: blue, $\mathbf{B_0}||\mathbf{Z}$: green).

populations (w_X, w_Y, w_Z) of zero-field are known, the populations (w_{+1}, w_0, w_{-1}) of high-field can be obtained as

$$w_\kappa(\Theta, \Phi) = \sum_\lambda |c_{\kappa\lambda}(\Theta, \Phi)|^2 w_\lambda \ (\kappa = 1, 0, -1; \lambda = X, Y, Z),$$
(6)

where $c_{\kappa\lambda}$ denotes the $\kappa\lambda$ element of the unitary matrix which diagonalize the Hamiltonian. In the case of the high field where the effect of ZFS can be negligible, the populations approach to

$$w_0 = w_X; \ w_{\pm1} = \frac{w_Y + w_Z}{2} \qquad \text{if } (\mathbf{B_0}||\mathbf{X}),$$
(7-1)

$$w_0 = w_Y; \ w_{\pm1} = \frac{w_Z + w_X}{2} \qquad \text{if } (\mathbf{B_0}||\mathbf{Y}),$$
(7-2)

$$w_0 = w_Z; \ w_{\pm1} = \frac{w_X + w_Y}{2} \qquad \text{if } (\mathbf{B_0}||\mathbf{Z}),$$
(7-3)

where $\mathbf{B_0}$ is the vector of the external magnetic field. In the case of pentacene, the polarization between w_0 and w_{+1} is maximized to 73% when $\mathbf{B_0}||\mathbf{X}$ according to imbalanced populations $(w_{+1}, w_0, w_{-1}) = (0.12, 0.76, 0.12)$.[65]

In a polycrystalline powder, the polarizing agents are randomly orientated, and its EPR spectrum is obtained as the sum of spectra with all angles Θ and Φ. It is possible to selectively use the polarizing agent in a specific orientation by tuning the magnetic field and microwave frequency for polarization transfer. When pentacene is used as the polarizing agent, the most efficient hyperpolarization can be achieved by using the condition in which the long axis is parallel to the external magnetic field ($\mathbf{B_0}||\mathbf{X}$, Fig. 4).

Polarization transfer and buildup

The polarization transfer from triplet electron spins to neighboring nuclear (typically ^{1}H) spins through ISE is achieved by the microwave irradiation under the magnetic field sweep. Due to the large (660 times) difference of gyromagnetic ratio γ between electron and nucleus, it is necessary to tune the

electron spin precession frequency in the rotating frame by applying the microwave to match the nuclear spin precession frequency in the laboratory frame (Fig. 5a). When these two frequencies match, the electrons and nuclei can exchange their spin states, i.e. the polarization transfer takes place.

In the laboratory frame, the electron spins process around the external magnetic field B_0 with the Larmor frequency ω_{e0} represented as

$$\omega_{e0} = -\gamma_e B_0,$$
(8)

where γ_e is the gyromagnetic ratio of electron spin. When the microwave with a frequency ω_{mw} is irradiated, the electron spins precess with a frequency $\omega_e = \gamma_e B_{eff}$ in the rotating frame around an effective magnetic field B_{eff} represented as

$$B_{eff} = \sqrt{\Delta B^2 + B_1^2},$$
(9)

where ΔB is the offset originating from the frequency difference between ω_{e0} and ω_{mw} ($\Delta B = (\omega_{e0} - \omega_{mw})/\gamma_e$), B_1 is the rotational magnetic field applied vertically to the external field B_0. In the rotating frame, B_1 behaves as a static magnetic field vertical to ΔB, and its strength is determined by the power of the applied microwave.

On the other hand, proton spins are off-resonant with the microwave and precess with a frequency $\omega_H = -\gamma_H B_0$ in the
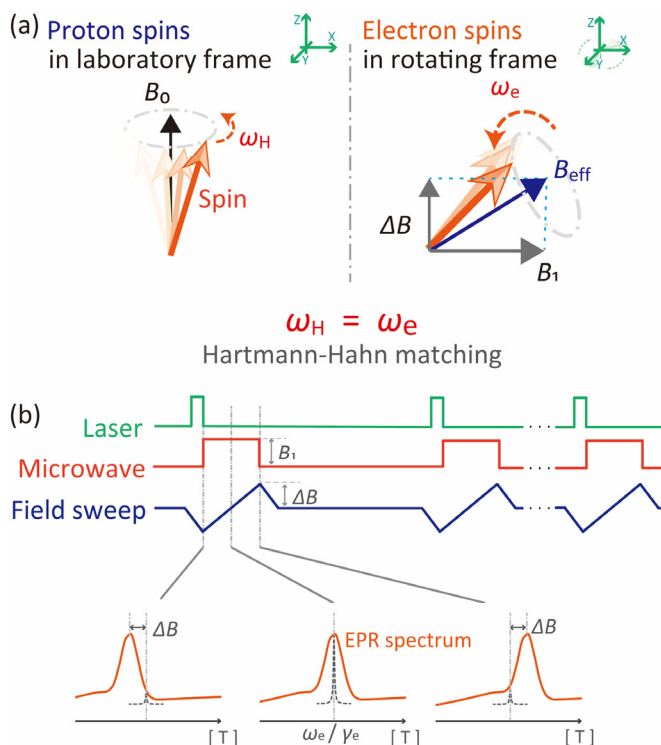
Fig. 5 (a) Precession of proton spin magnetization vector in the laboratory frame (left) and electron spin in the rotating frame (right). When ω_H becomes equal to ω_e, the polarization transfer occurred most efficiently (Hartmann-Hahn matching condition). (b) Scheme of triplet-DNP sequence. The pulsed photoexcitation is followed by microwave irradiation and magnetic field sweep, which is repeated before the NMR measurement. By the adiabatic magnetic field sweep, all the spin packets in the swept range can participate in the polarization transfer through ISE.

laboratory frame. By choosing ΔB and B_1, the frequency ω_e can be changed to become equal to ω_H, the so-called Hartmann-Hahn matching condition

$$\gamma_H B_0 = \gamma_e B_{eff}, \tag{10}$$

in which electrons and nuclei can exchange the spin states with each other like resonance between pendulums connected by springs. The springs in the coupled pendulums correspond to the "flip-flop" term of the dipolar interaction in the spin systems.

Since the EPR linewidth is broadened by hyperfine coupling (and different molecular orientations in a polycrystalline powder), and therefore it is impossible to satisfy the Hartmann-Hahn condition for all spin packets simultaneously. To solve this issue, Wenckebach and coworkers applied the ISE technique that uses the external magnetic field sweep over the full EPR linewidth under the continuous microwave irradiation (Fig. 5b).[61] All the electron spin packets in the swept range can participate in the polarization transfer. The field sweep rate has to be sufficiently slow compared with the effective precession frequency to satisfy the adiabatic condition. The lifetime of photo-excited triplet electron polarization should be long enough (> a few microseconds) to satisfy the adiabatic condition.

The polarization transfer is followed by the diffusion of nuclear (^1H) spin polarization. The spin diffusion occurs through the "flip-flop" term of the dipolar interaction of homonuclear spins. In typical samples with a lot of protons, the spin diffusion is faster than the DNP repetition rate, and the buildup rate of proton polarization is independent of the spin diffusion rate. The time evolution of proton polarization P can be calculated from DNP repetition rate R and spin-lattice relaxation rate as

$$\frac{d}{dt}P(t) = R\eta\xi\frac{\rho_e}{\rho_H}[P_e - P(t)] - \frac{1}{T_1'}[P(t) - P_{th}]$$

$$\sim R\eta\xi\frac{\rho_e}{\rho_H}[P_e - P(t)] - \frac{1}{T_1'}P(t), \tag{11}$$

where η is the fraction of the triplet electron spins in the two triplet sublevels involved in the polarization transfer, ξ is the exchange probability, ρ_e and ρ_H are densities of electron and proton spins, P_e is the polarization of electron spins, T_1' is spin-lattice relaxation time of ^1H under the laser irradiation, and P_{th} is the polarization of proton spins in thermal equilibrium that is negligibly small compared with P. Tateishi et al. noticed that the triplet electrons of the polarizing agent induce the spin-lattice relaxation of neighboring ^1H spins through the perturbation of the local field of the ^1H spins.[79] Therefore, T_1' includes the 2 components, ^1H spin-lattice relaxation time without laser irradiation (T_1) and that in the presence of photo-excited triplet electrons (T_{1e}), as

$$\frac{1}{T_1'} = \frac{1}{T_1} + \frac{1}{T_{1e}}. \tag{12}$$

The solution of the above eq. 11 is given by

Fig. 6 Scheme of the setup for triplet-DNP. PA is power amplifier, MW osc is microwave oscillator, FG is function generator, trig. is TTL trigger signal, and LNA is low noise amplifier.

$$P(t) = \frac{P_e}{1 + T_b/T_1'}\left[1 - exp\left\{-t\left(\frac{1}{T_b} + \frac{1}{T_1'}\right)\right\}\right] \tag{13}$$

$$T_b = \frac{\rho_H}{R\eta\xi\rho_e}, $$

where T_b is buildup time constant. The maximum polarization is obtained as

$$P_{max} = \frac{P_e}{1 + T_b/T_1'}. \tag{14}$$

Therefore, the long T_1 value is crucial to achieve the high nuclear polarization.[64, 69, 70, 79]

Experimental setup of triplet-DNP

Here we take our experimental setup of triplet-DNP as an example (Fig. 6). Triplet-DNP is carried out using a Ku-band cylindrical resonator with a window for laser irradiation and a coil for the magnetic field sweep at a magnetic field generated by an electromagnet. The external magnetic field B_0 is set at around 0.67 T, in which ^1H and triplet electron spins of pentacene resonate at ca. 28 MHz and 17.7 GHz, respectively. A sample is put in Pyrex/quartz/sapphire tubes and set in the cavity. A pulsed laser was used for the excitation of the polarizing agent. For pentacene, the typical wavelength, pulse width, pulse energy, and repetition rate are 500~600 nm, > 100 ns, > 0.1 mJ, and 10~1,000 Hz, respectively. A microwave is generated and amplified using pulsed TWTA (Traveling Wave Tube Amplifier) up to 2 kW (Hartmann-Hahn condition can be satisfied at ~50 W). A triangle wave for field sweep is produced with a function generator and amplified with OPamp. After triplet-DNP, the polarized sample is shuttled into an NMR coil positioned above the resonator, which is tuned for ^1H. The timing control of the ISE sequence and the NMR detection are performed with an OPENCORE NMR spectrometer.[99]

3. Nanomaterials for in-situ triplet-DNP

While the advantage of triplet-DNP is its high working temperature compared with radical-based DNP, the polarizable matrix (host material) had been limited to dense molecular crystals such as *p*-terphenyl and naphthalene at room

temperature. This is mainly because the polarizing agent had been limited to pentacene and only these molecular crystals can accommodate pentacene molecules without aggregation. Besides, the use of dense molecular crystals was necessary to suppress molecular motions for the long spin-lattice relaxation time T_1. Unfortunately, most of biology-relevant substances and water cannot be accommodated in the dense crystals to be polarized. To overcome this situation, our group has proposed the concept of "increasing the surface area" while keeping the structural rigidity of the matrix. This new concept would realize the polarization transfer from the rigid matrices to target compounds through the optimization of the interaction between the matrix and target at their interface, towards our final goal of in-situ triplet-DNP at room temperature.

Metal-organic frameworks (MOFs) as nanoporous matrices

One of our strategies of increasing the surface area is to employ nanoporous materials with great accessibility for polarizing targets. Among various nanoporous materials, we chose metal-organic frameworks (MOFs) since MOFs offer not only rigid crystalline structures but also significant structural and functional tunability that should be beneficial to optimize the host-guest interaction and to establish the design guideline of polarization transfer to various guest molecules of interest. Note that recent pioneering works on low-temperature radical-based DNP have shown the potential benefits of porous materials to polarize some guest molecules,[100-108] there was no example of room-temperature DNP using porous matrices.

For the proof-of-concept, we have reported the first example of triplet-DNP of prototypical diamagnetic Zn^{2+}-based MOF, $[Zn(MeIM)_2]_n$ (ZIF-8; MeIM = 2-methylimidazolate).[109] We synthesized a novel polarizing agent by modifying the typical polarizing agent pentacene with metal-coordinating carboxylate moieties ((4,4'-(pentacene-6,13-diyl)dibenzoic acid (PDBA), Figure 7b) for its introduction into MOFs. The PDBA molecules were successfully accommodated during the crystallization of ZIF-8 in methanol in the presence of NaOH at room temperature. The fact that a nonionic pentacene derivative 6,13-diphenylpentacene (DPP) was not incorporated into ZIF-8 suggests the important role of the coordination of carboxylate moieties to Zn^{2+} ions of ZIF-8 for the accommodation of PDBA. Since the aggregation of polarizing agent induces the relaxation of electron spin polarization, the crystallization condition was optimized to achieve the good dispersibility of PDBA in ZIF-8, which was confirmed by UV-Vis and fluorescence measurements.

It was found that the partial deuteration of ligands successfully elongates the ^1H T_1 of MOF. The ^1H T_1 value of ZIF-8 was estimated as 31 ± 0.1 s at room temperature (Fig. 7c). We assumed the rotation of methyl groups in ZIF-8 caused the spin-lattice relaxation to decrease the ^1H T_1 value and synthesized a partially deuterated ligand to construct methyl-deuterated ZIF-8 (denoted as D-ZIF-8). As expected, D-ZIF-8 successfully
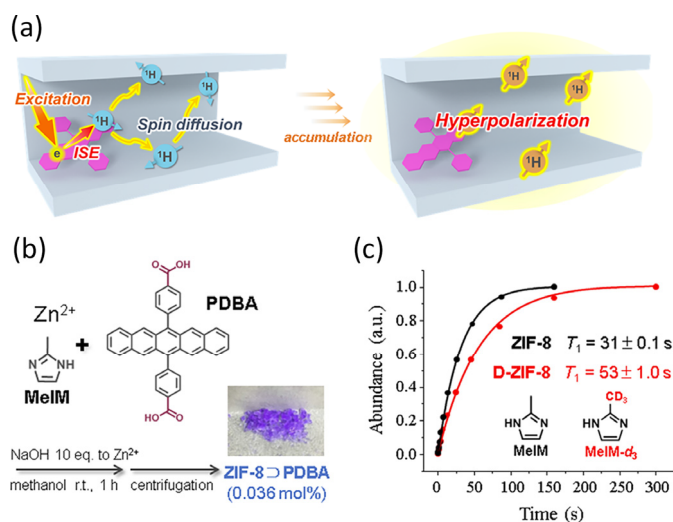
Fig. 7 (a) Schematic illustration of triplet-DNP in MOFs accommodating polarizing agents. (b) Synthetic scheme and a photograph of ZIF-8⊃PDBA. (c) ^1H spin–lattice relaxation (T_1) data of ZIF-8 (black) and D-ZIF-8 (red) acquired with the saturation-recovery sequence. Adopted with permission from ref. 109. Copyright 2018 American Chemical Society.

showed a longer ^1H T_1 value of 53 ± 1.0 s. The inclusion amount of PDBA inside D-ZIF-8 was optimized based on the intensity of the time-resolved EPR signal of the photoexcited triples. Note that the ^1H T_1 value of ZIFs was not significantly affected by the incorporated 0.036 mol% of PDBA.

The transfer of spin polarization from photoexcited triplet electrons of PDBA to ^1H nuclei of D-ZIF-8 was carried out with the ISE sequence. The PDBA molecules inside D-ZIF-8 were photoexcited by a pulsed 589 nm laser (500 Hz), followed by a microwave irradiation (18.1 GHz) and a field sweep (±100 G). The duration of microwave irradiation (10 μs) was optimized based on the enhancement of the ^1H NMR signal intensity. After repeating this process to accumulate the spin polarization, ^1H NMR spectra were immediately measured. The ^1H NMR signal intensity of D-ZIF-8 containing polarizing agents showed a large enhancement factor of 58, and the signal-to-noise ratio of ^1H NMR spectra was significantly improved by the triplet- DNP process (Fig. 8a, b). The triplet-DNP process was also carried out at a lower temperature (220 K), which is relevant to the adsorption of the ^{129}Xe gas probe. As a result, 85 and 102 times enhancement were achieved compared to the thermal equilibrium at 220 K and room temperature, respectively. A longer buildup time constant T_b of 13 s at 220 K than that at room temperature (8.5 s) indicates that the increase in the ^1H NMR signal enhancement at the lower temperature is mainly due to the reduced molecular mobility and prolonged ^1H T_1. Note that the pentacene derivative PDBA in D-ZIF-8 was found to be not stable in repeated long-term laser irradiation. This problem can be solved by employing diaza-substituted polarizing agents with improved stability as described in a later section. The above results proved the new concept of using MOFs as 'porous' and 'rigid' hosts for triplet-DNP, and the polarization transfer from MOFs to guest molecules of interest is an obvious next step. Given the structural and functional diversity, we believe that MOFs will
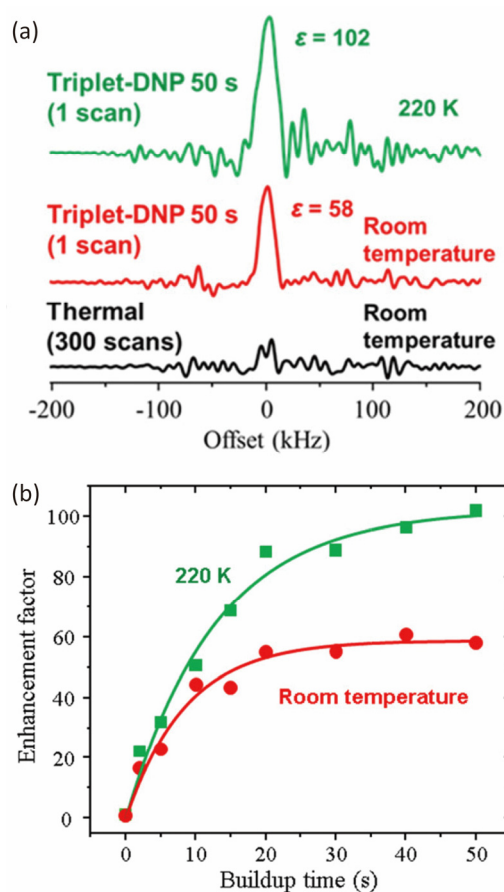
Fig. 8 (a) ^{1}H NMR signals of D-ZIF-8⊃PDBA under thermal equilibrium (300 scans every 3 min) and after triplet-DNP (ISE sequence for 50 s and 1 scan) at room temperature and 220 K. (b) ^{1}H polarization buildup curve of D-ZIF-8⊃PDBA at room temperature and 220 K. Adopted with permission from ref. 109. Copyright 2018 American Chemical Society.

Fig. 9 (a) Schematic representation of downsizing bulk crystals to nanocrystals for triplet-DNP in water. (b) Chemical structures of pentacene (polarizing agent) and p-terphenyl (crystalline matrix). Bulk crystals of p-terphenyl doped with 0.5 mol% pentacene were ball-milled in an aqueous solution of CTAB (1.4 mM), resulting in an aqueous dispersion of nanocrystals. (c) SEM image of the nanocrystals. (d) DLS profile of the aqueous dispersion of nanocrystals. Adopted with permission from ref. 110. Copyright 2019 The Royal Society of Chemistry.

serve as an applicable room-temperature hyperpolarization system for a wide range of target molecules.

Triplet-DNP of nanocrystals dispersed in water

The application of triplet-DNP had been limited to the solid-state. This is mainly because the effective ISE and the accumulation of spin polarization through spin diffusion require the solid crystals with long spin-lattice relaxation time T_1. Besides, paramagnetic oxygen molecules severely quench the photo-excited triplet state. Therefore, it was not clear whether it is possible to achieve triplet-DNP in water containing dissolved oxygen molecules.

Our group has demonstrated the first example of triplet-DNP in water by downsizing the conventional bulk crystals to nanocrystals (Fig. 9a).[110] This was also the first example of triplet-DNP of nanosized crystals. As a proof-of-concept, pentacene and p-terphenyl were employed as benchmark polarizing agent and crystalline matrix, respectively (Fig. 9b). A stable nanocrystal dispersion in water was obtained by a simple ball-milling process. Bulk p-terphenyl crystals doped with 0.5 mol% pentacene in an aqueous solution of cetyltrimethylammonium bromide (CTAB) were ball-milled for 3 hours to provide a purple milky suspension (Fig. 9b). The size of the obtained particles was around 100 nm (Fig. 9c, d). The

good colloidal stability was achieved by the surface coverage of nanoparticles with the cationic CTAB surfactant. The maintenance of good crystallinity after the ball-milling process was confirmed by the unchanged powder X-ray diffraction (PXRD) peak width.

Importantly, the triplet state of pentacene is well protected in the dense p-terphenyl crystal structure from the oxygen quenching even in the form of nano-sized crystals (Fig. 10b). Transient absorption measurements showed that the triplet lifetime of pentacene in the nanocrystals is identical to that in the bulk crystals, showing the good oxygen blocking ability of the p-terphenyl nanocrystals (Fig. 10a).

In-water triplet-DNP was demonstrated by applying the ISE sequence to the aqueous dispersion of the nanocrystals in the ambient condition. After a pulsed laser excitation at 532 nm, the electron spin polarization was transferred to ^{1}H spins by the microwave irradiation (17.7 GHz, <300 W) under the magnetic field sweep (676 mT ± 30 mT), and the triplet-DNP process was repeated for a certain duration before the ^{1}H-NMR measurements. Without the triplet-DNP process, only a sharp NMR peak from the water was observed due to the weak and broad signal of nanocrystals (Fig. 10c). Significantly, the intensity of the broad peak from nanocrystals gradually
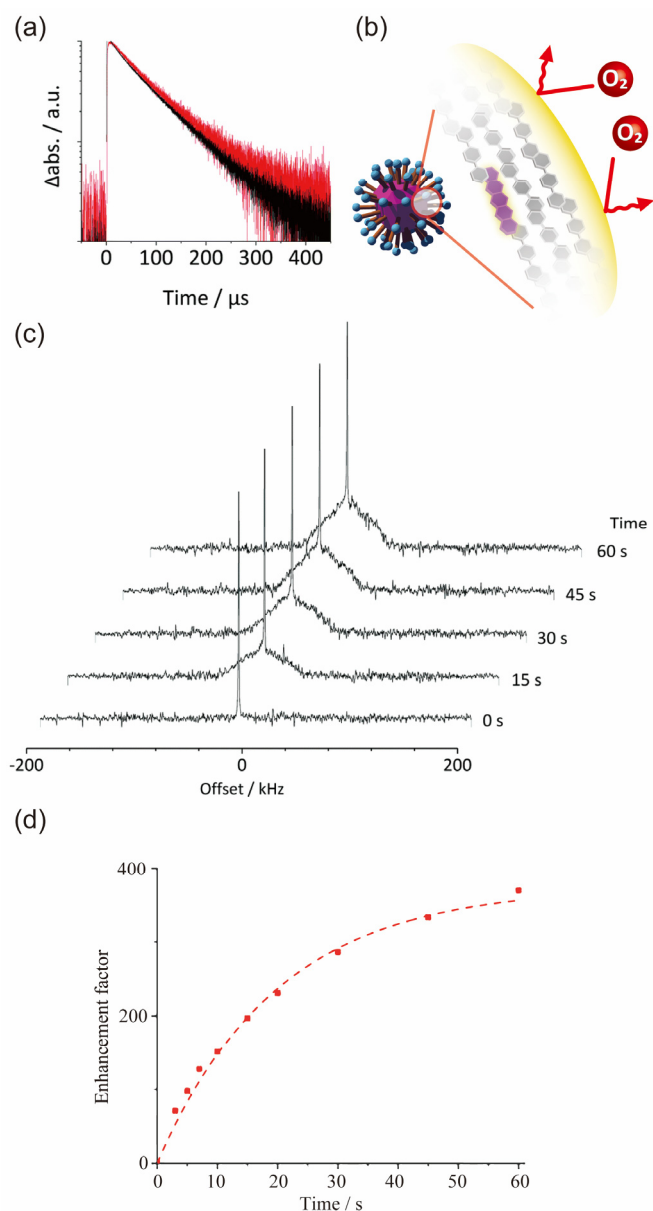
Fig. 10 (a) Transient absorption intensity of bulk *p*-terphenyl crystals doped with 0.5 mol% pentacene (black) and the aqueous dispersion of *p*-terphenyl nanocrystals doped with 0.5 mol% pentacene (red). (b) Schematic illustration of oxygen blocking in the nanocrystals. The photo-excited triplet state of pentacene is protected from oxygen quenching thanks to the dense matrix structure. (c) ^{1}H NMR spectra (0.676 T) of the aqueous dispersion of *p*-terphenyl nanocrystals doped with 0.5 mol% pentacene at the thermal equilibrium and after the triplet-DNP process for different durations at room temperature in air. (d) ^{1}H polarization buildup curve of the aqueous dispersion of *p*-terphenyl nanocrystals doped with 0.5 mol% pentacene at 0.676 T and room temperature. The broken line is a fitting curve with the following equation, $A[1-exp(-t/T_B)]$. Adopted with permission from ref. 110. Copyright 2019 The Royal Society of Chemistry.

increased by elongating the triplet-DNP duration, and the enhancement factor reached over 360 times (0.083%, Fig. 10d). The future optimization of the nanocrystal surface structure would enable the polarization transfer from nanocrystals to surrounding water molecules, leading to selective hyperpolarization of solvent-exposed residues of proteins through proton exchange at the ambient condition.

4. Dissolution triplet-DNP

Dissolution-DNP using radical electrons is currently the most powerful method to achieve the hyperpolarized state in a solution for NMR and MRI applications. However, the radical-based dissolution-DNP requires the cryogenic temperature (~1 K) and the high magnetic field (>3 T) with a superconducting magnet. The implementation of the dissolution process to room-temperature triplet-DNP at the low magnetic field (< 1 T) can be a complementary low-cost hyperpolarization method for the wide use.

Negoro et al. have reported the first example of dissolution triplet-DNP by doping pentacene into a water-soluble crystalline matrix, benzoic acid.[111] To elongate the ^{1}H spin-lattice relaxation time T_1 and to suppress the proton relaxation induced by triplet electrons, partially-deuterated benzoic acid (BA-d_1) and fully deuterated pentacene-d_{14} were employed. For a powder sample of BA-d_1 doped with 0.04 mol % pentacene-d_{14}, a ^{1}H spin polarization of 0.8% was achieved after performing the triplet-DNP process for 10 min at room temperature. By injecting a 1M hot deuterated solution of sodium carbonate to the hyperpolarized powder, a broad NMR signal of the solid powder turned into a sharp peak (Fig. 11a). Interestingly, the areas of these broad and sharp NMR spectra were almost the same, suggesting the retention of polarization during the dissolution process.

Kagawa et al. have extended the dissolution triplet-DNP to high-field ^{13}C NMR by employing [carboxy-^{13}C]benzoic acid-*d* (BA1d) as a crystalline matrix.[112] After triplet-DNP of pentacene-doped BA1d powder, the high polarization of ^{1}H spins were
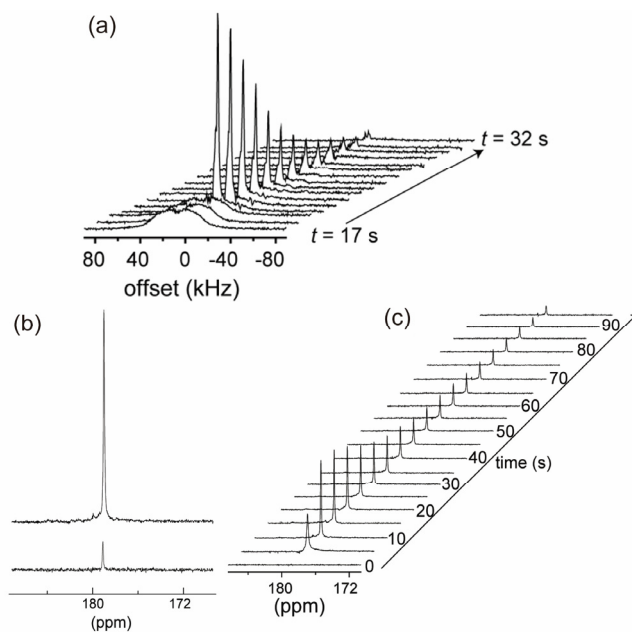
Fig. 11 (a) ^{1}H NMR spectra of BA-d_1 in dissolution triplet-DNP. A hot aqueous solution was injected 20 s after triplet-DNP, while the ^{1}H magnetization was measured with 15° pulses repeatedly at intervals of 1 s. Time *t* is the interval from just finishing triplet-DNP to the NMR measurement. (b) Solution ^{13}C NMR spectra at 11.7 T of BA1d at the thermal equilibrium (bottom, 64 times accumulation) and after dissolution triplet-DNP (top). (c) Time-resolved enhanced solution ^{13}C NMR spectra of BA1d. Adopted with permission from ref. 111 and 112. Copyright 2018 American Chemical Society, 2019 Elsevier.
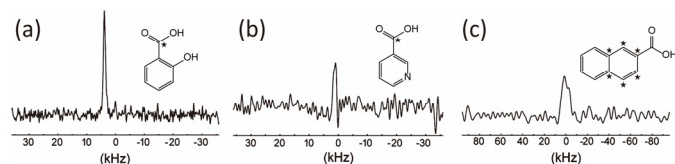
Fig. 12 Enhanced ^{13}C NMR spectra of mixtures of benzoic acid-d_6 and (a) [carboxy-^{13}C]salicylic acid, (b) [carboxy-^{13}C]nicotinic acid, and (c) 2-naphthoic acid-^{13}C$_6$ by triplet-DNP and RAMP-CP at 0.39 T and room temperature. Adopted with permission from ref. 113. Copyright 2018 American Chemical Society.

transferred to ^{13}C spins by a ramped amplitude cross-polarization (RAMP-CP) at 0.39 T. The ^{13}C-polarized sample was manually shuttled to an 11.7 T superconducting magnet and dissolved by a hot sodium hydroxide solution in D$_2$O. As a result, a highly enhanced ^{13}C MMR signal of BA1d was observed, and the enhancement factor was estimated as 220, corresponding to ^{13}C polarization of 0.22% (Fig. 11b). Reflecting the long relaxation time of carboxyl ^{13}C spin in BA1d (48 s), the enhanced ^{13}C NMR signal was observed for more than 1 min (Fig. 11c).

While the high polarization of benzoic acid was successfully obtained, it was difficult to extend the same strategy to other water-soluble compounds due to the poor dispersibility of pentacene. To overcome this limitation, Kagawa et al. have proposed a strategy of making eutectic mixtures of benzoic acid and another target compound such as salicylic acid, nicotinic acid, and 2-naphthoic acid.[113] Pentacene was successfully doped in the 1:1 mixture of benzoic acid-d_6 and one of the target compounds (salicylic acid-d_2, nicotinic acid-d_1, or 2-naphthoic acid). Triplet-DNP of the pentacene-doped mixtures resulted in high ^{1}H polarizations of 1.2%, 0.33%, and 0.36% for salicylic acid-d_2, nicotinic acid-d_1, or 2-naphthoic acid, respectively. Using ^{13}C-labeled target compounds, the enhanced ^{1}H polarization of the mixtures were transferred to ^{13}C spins using the RAMP-CP sequence. While no ^{13}C signals were obtained at the thermal equilibrium in 0.39 T, enhanced ^{13}C signals were observed after the triplet-DNP and RAMP-CP processes (Fig. 12).

Despite these initial successes, the variety of polarizable compounds by dissolution triplet-DNP is still limited to benzoic acid and its eutectic mixtures due to the strong hydrophobic and aggregation nature of pentacene. Benzoic acid is rather exceptional since the hydrogen-bonded benzoic acid dimer has a similar size and shape of pentacene and thus can accommodate pentacene without aggregation in its crystal structure.[114] Besides, the degradation of pentacene under long-time photoexcitation was also observed.[113] We envisage that the applicability of dissolution triplet-DNP would be significantly widened by the development of non-pentacene derivatives with better solubility and stability mentioned below.

5. Novel polarizing agents

Since the first demonstration of effective room-temperature triplet-DNP by Wenckebach et al. in 1990, pentacene had been the only and best polarizing agent for triplet-DNP. This is partly because pentacene has the high electron polarization, its electron polarization (transient EPR)

lifetime is long enough for polarization transfer, and its triplet (transient absorption) lifetime is not too long to induce the nuclear spin-lattice relaxation. Besides, the polarizing agent should be doped without aggregation in crystalline matrices with long ^{1}H T_1 such as p-terphenyl and naphthalene. Pentacene has the ideal molecular shape and size for this purpose since one pentacene molecule can be substituted with one p-terphenyl molecule or two naphthalene molecules in their crystal structures. Therefore, it is reasonable to employ pentacene for the application of triplet-DNP in nuclear physics experiments using large single crystals.

However, pentacene is far from ideal when it comes to biological applications. Pentacene decomposes within a few minutes in solution in the ambient conditions and its dispersibility is extremely low in water and biology-relevant hydrophilic substances. Furthermore, the photo-stability of pentacene is not enough for prolonged pulse excitation in some matrices.[109, 113] The development of polarizing agents with better stability and solubility is crucial to expand the scope of triplet-DNP.

Pentacene derivatives with improved solubility

The solubility issue of pentacene can be circumvented by using substituted pentacene derivatives. For example, PDBA could be introduced into D-ZIF-8 thanks to its good solubility in organic solvents (Fig. 7b).[109] Tateishi et al. have reported the first demonstration of triplet-DNP in the glass state of organic
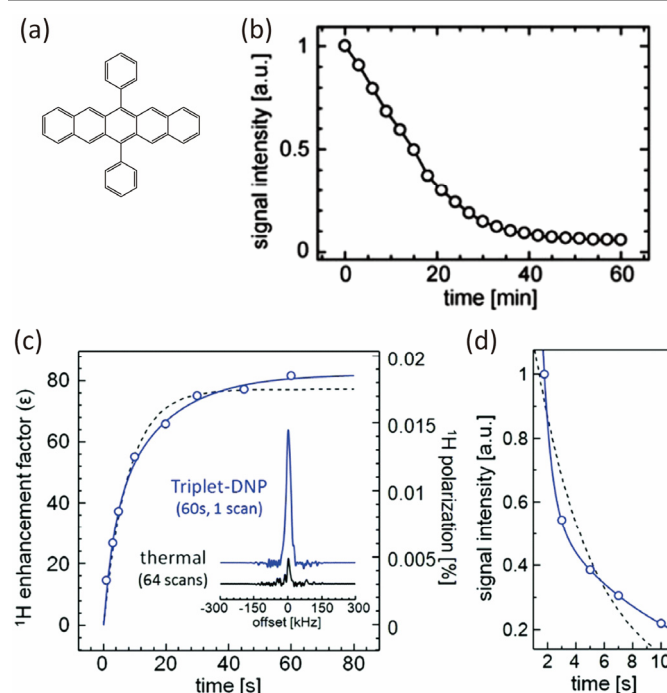
Fig. 13 (a) Structure of 6,13-diphenylpentacene (DPP). (b) Time dependence of absorption intensity at 594 nm. The sample was exposed to ambient light and air. (c) Buildup curve of the ^{1}H signal in the glass of ethanol-d_6 : water = 80 : 20 (w/w) doped with 0.1 mM DPP at 90 K and in 0.6673 T. (inset) The ^{1}H NMR spectra of the polarized and thermally-equilibrated sample. (b) T_1 measurement by changing the interval from triplet-DNP to NMR measurement. The data are fit with bi/mono-exponential functions (the solid/dashed lines). Adopted with permission from ref. 115. Copyright 2019 The Royal Society of Chemistry.

solvent by employing the pentacene derivative DPP (Fig. 13a).[115] DPP is soluble in common organic solvents such as chloroform, DMSO, toluene, and alcohols. DPP was dissolved in ethanol-d_6, and subsequently, 20 wt% of water was added. The obtained solution was solidified by brewing cold N_2 gas. Time-resolved EPR measurements of DPP in ethanol-d_6/water glass at 120 K showed that the zero-field splitting parameters and polarization of DPP were similar to those of pentacene.[65, 79, 116] The triplet-DNP process was carried out for 0.1 mM DPP in the glass of ethanol-d_6 : water = 80 : 20 (w/w) at 90 K, resulting in the 81 times enhancement of water ^{1}H signal (Fig. 13c). This moderate polarization was attributed to the short T_1 (0.60 s (45%) and 8.8 s (55%)) of the glass matrix as well as the low DPP concentration for preventing the sample heating under the laser and microwave irradiation. Both buildup and relaxation curves cannot fit with mono-exponential function and can fit with bi-exponential function (Fig. 13c, d). This implies that the sample condition gradually changed upon generation of heat by the laser and microwave irradiation.

While the solubility was significantly improved by the functionalization of pentacene, the stability issue remains. In the ambient light and air, DPP was decomposed with a half-lifetime of 15 min (Fig. 13b). During the sample preparation (dissolution of DPP and solidification of the solution by cooling) of ~5 min, ~20% of DPP was decomposed. A new molecular design can solve this problem as mentioned below.

Non-pentacene polarizing agents with improved air-stability

Pentacene and its derivatives suffer from their poor stability in air. To overcome this issue, our group has reported air-stable polarizing agents with high polarization ability comparable to pentacene for the first time.[116] The new and simple molecular design, aza-substituted acenes, was demonstrated to be promising by taking 6,13-diazapentacene (DAP) and 5,12-diazatetracene (DAT) as examples. The introduction of electron-withdrawing nitrogen atoms to pentacene and tetracene reduces both highest occupied molecular orbital (HOMO) and lowest unoccupied molecular orbital (LUMO) energy levels, as confirmed by density functional theory (DFT) calculations (Fig. 14a). The lower HOMO and LUMO energy levels of DAP and DAT suggest their higher stability under ambient conditions by suppressing the photooxidation in the ground and excited states. The stability of the triplet polarizing agents was experimentally verified by measuring the time-dependent UV-vis absorption spectra of DAP and DAT in THF under the ambient condition (Fig. 14b, c). The diaza-substitution significantly suppressed the decomposition of DAP and DAT compared with pentacene and tetracene, respectively.

Remarkably, the potential of DAP and DAT as triplet polarizing agents was found to be comparable to pentacene. 0.05 mol% of each polarizing agent was doped in host crystalline powders of *p*-terphenyl. Time-resolved EPR measurements showed that the spin polarizations in the triplet excited state of DAP (49%) and DAT (66%) are comparable to that of pentacene (73%). The main components of EPR decay time were 18, 3.1, and 11 μs for pentacene, DAP, and DAT, respectively. After
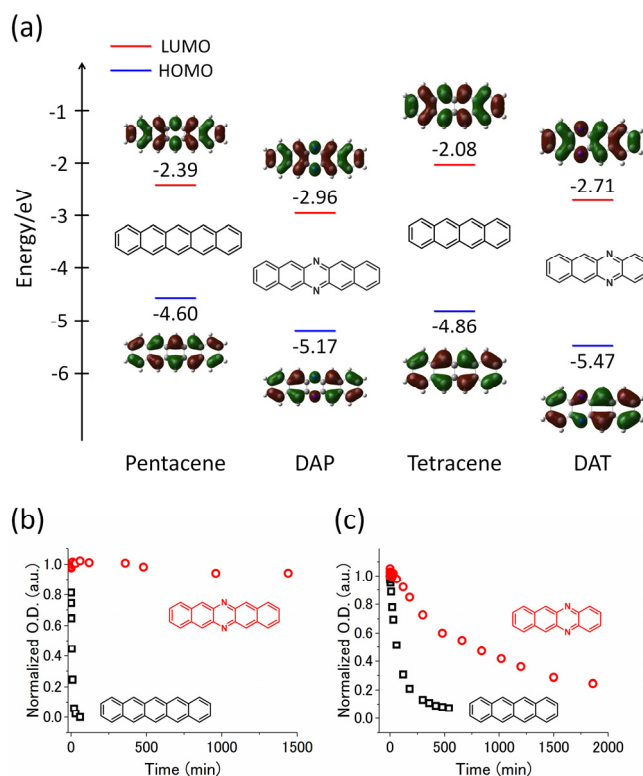
Fig. 14 (a) HOMO and LUMO energy levels of pentacene, DAP, tetracene, and DAT at the B3LYP/6-31G(d) level. (b) Time dependence of optical density (O.D.) at the absorption peak of pentacene (575 nm) and DAP (640 nm) in THF under the air-saturated and ambient light conditions. (c) Time dependence of optical density (O.D.) at the absorption peak of tetracene (473.5 nm) and DAT (500 nm) in THF under the air-saturated and ambient light conditions. Adopted with permission from ref. 116. Copyright 2019 American Chemical Society.
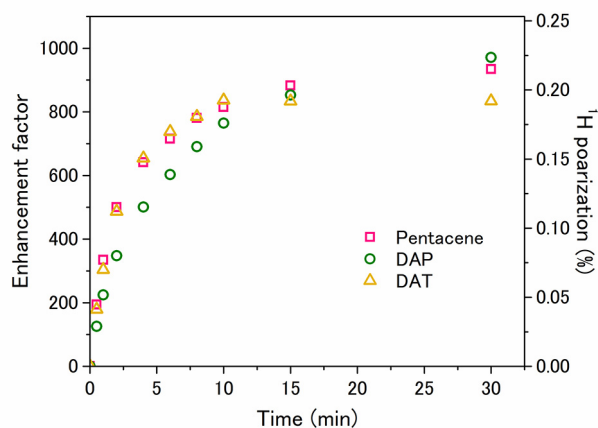
Fig. 15 ^{1}H polarization buildup curves of *p*-terphenyl crystalline powders doped with 0.05 mol % of pentacene (pink, 0.676 T), DAP (green, 0.678 T), and DAT (yellow, 0.682 T) at room temperature using a 18.2 GHz cylindrical resonator. The sweep width of the magnetic field for polarization transfer was ±30 mT. Adopted with permission from ref. 116. Copyright 2019 American Chemical Society.

triplet-DNP, the high ^{1}H spin polarization of 0.22% and 0.19% were obtained for DAP- and DAT-doped *p*-terphenyl, respectively, which were comparable to that of pentacene-doped *p*-terphenyl (0.21%) in the identical experimental

condition (Fig. 15). The long polarization lifetime of pentacene had been considered to be requisite for the efficient polarization transfer, but importantly, a few µs of polarization lifetime was revealed to be long enough from the triplet-DNP experiments using DAP. This finding motivates the further exploration of new polarizing agents even other than the acene family.

Water-soluble triplet polarizing agents

Water is a ubiquitous polarization source; the water hyperpolarization can be transferred to biomolecules such as amino acids, peptides, and proteins through proton exchange, as demonstrated in radical-based dissolution-DNP.[117-120] The key to achieving the water hyperpolarization at a higher temperature is to utilize the long T_1 of ^1H in crystalline ice over 5 minutes. However, there have been no reports on water-soluble polarizing agents, and it was required to use the ethanol-d_6/ water mixture with the short $T_1 < 10$ s for dissolving the pentacene derivative DPP.[115]

Our group has reported the first example of a water-soluble triplet polarizing agent as well as the first demonstration of triplet-DNP of crystalline ice.[121] By taking advantage of the high air-stability of DAT, a novel water-soluble triplet polarizing agent DAT-4COOH having four carboxylic acid groups was synthesized (Fig. 16). Spectroscopic studies showed that a sodium salt of DAT-4COOH (DAT-4COONa) aggregates in crystalline ice at 140 K. In stark contrast, an ion-pair of DAT-4COOH with a hydrophilic and bulky cation MEEA (Fig. 16)[122] could be dispersed in crystalline ice without aggregation. DAT modified with a fewer number (two) of carboxylic acid moieties (DAT-2COOH) could not be dispersed in ice even after forming the ion complex with MEEA, indicating that it is important to introduce the enough number of ion-pairs to prevent the chromophore aggregation. The absence of a significant effect on photo-excited triplet polarization by the hydrophilic modification of DAT was confirmed by time-resolved EPR measurements. DAT-4COOH/MEEA in water at 140 K showed similar zero-field splitting parameters and relative zero-field populations to those of DAT in p-terphenyl.

The triplet-DNP process was carried out for water doped with DAT-4COOH/MEEA at 140 K in 0.664 T. An enhancement factor of 23 was obtained for ^1H NMR signal of water after the triplet-DNP sequence for 65 min (Fig. 17). Importantly, the long buildup time clearly indicated that the ^1H hyperpolarization was accumulated in crystalline ice with long T_1.[115] This moderate polarization enhancement might be due to the disorder of ice crystals around the DAT-4COOH/MEEA ion pair that induces the relaxation of nuclear polarization. In addition, the quantum yield of triplet formation through ISC was found to be lower than 23% for DAT-4COOH/MEEA in ice at 77 K. While further improvement of enhancement factor is necessary towards the actual NMR and MRI applications, the first example of triplet-DNP of crystalline water was achieved by molecularly dispersing the water-soluble polarizing agent with the help of bulky hydrophilic counter cation.
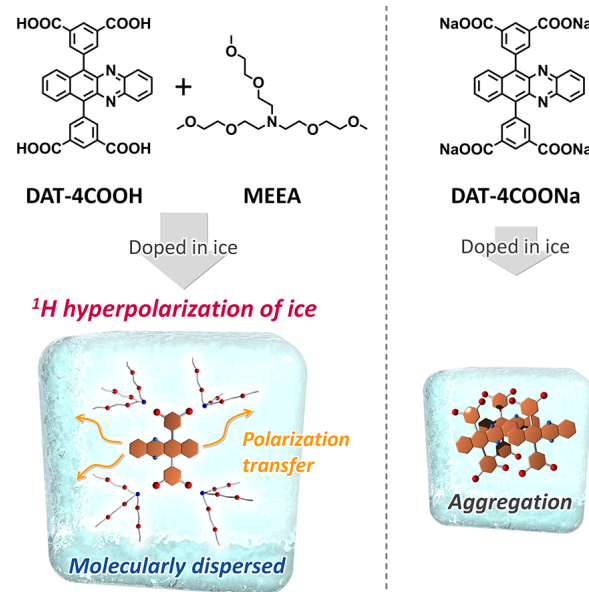
Fig. 16 Schematic illustration of aggregation-free dispersion of the ion pair between DAT-4COOH and MEEA for triplet-DNP of crystalline ice. DAT-4COONa aggregates in crystalline ice. Adopted with permission from ref. 121. Copyright 2020 the Royal Society of Chemistry.
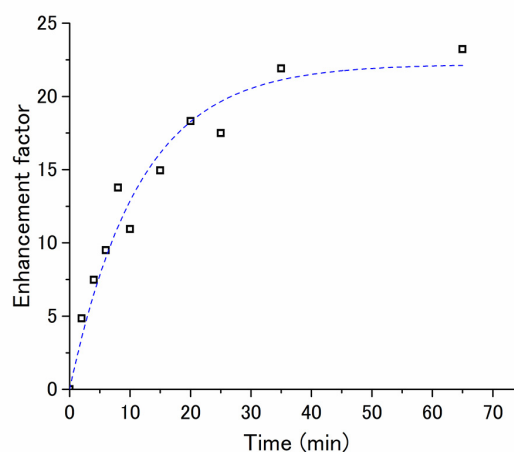
Fig. 17 Buildup curve of the ^1H NMR signal of DAT-4COOH/MEEA in water at 140 K and 0.664 T. The sweep width of the magnetic field for polarization transfer was ±30 mT. The broken line is a fitting curve with the following equation, A[1-exp(-t/T_B)]. Adopted with permission from ref. 121. Copyright 2020 the Royal Society of Chemistry.

6. Conclusion and Outlook

New possibilities of triplet-DNP have emerged by the recent introduction of materials chemistry. While the significantly high nuclear polarization had been achieved by triplet-DNP of the large single crystal, its application has been limited to nuclear physics experiments. The development of the new materials chemistry concepts overviewed here, such as nanoporous MOFs, nanocrystals, dissolution triplet-DNP, and air-stable and water-soluble polarizing agents, would maximize the potential of triplet-DNP at room-temperature and low magnetic field, paving new ways towards biological and medical applications.
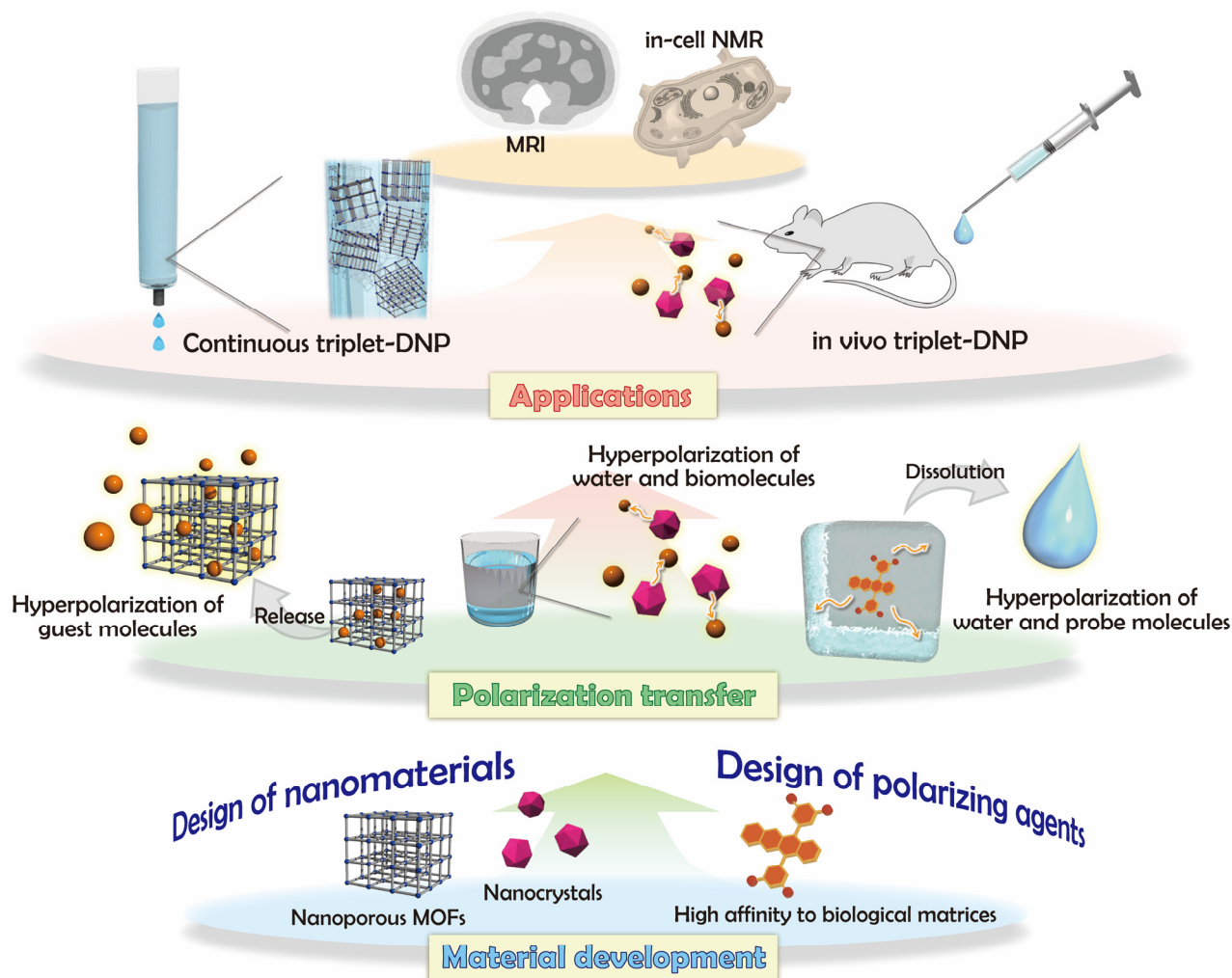
Fig. 18 Schematic illustration of triplet-DNP research stages toward biological applications. Recently, material development has been reported and researchers engaged in the polarization transfer step. When the polarization transfer step is attained, the way to practical applications, such as in cell NMR and MRI, is opened.

To make triplet-DNP more accessible, the nanostructured materials with large surface area such as nanoporous MOFs and nanocrystals were employed. These nanomaterials were successfully hyperpolarized by triplet-DNP at room temperature thanks to the relatively long T_1 values of the rigid structures. While the enhancement factor of these nanomaterials needs to be improved, these materials have the potential to realize the unconventional *in situ* triplet-DNP systems. MOFs are expected to transfer its hyperpolarization to guest target compounds and release the hyperpolarized molecules. Based on this hyperpolarization nanospace concept, a continuous supply of a hyperpolarized solution is anticipated (Fig. 18). If the polarization transfer from nanocrystals to surrounding water is succeeded, *in-vivo* triplet-DNP of biomolecules such as metabolites, lipids, peptides, and proteins through proton exchange with hyperpolarized water becomes reality (Fig. 18).

The dissolution triplet-DNP at room-temperature has an advantage in terms of instrumental cost compared with the common radical-based dissolution-DNP. The hyperpolarization of biologically relevant molecules such as benzoic acid and nicotinic acid were hyperpolarized without gyrotron and cryogen. At this moment the successful examples of dissolution triplet-DNP have been limited to benzoic acid and its eutectic mixtures mainly due to the poor dispersibility of pentacene. By combining the recent advances of novel polarizing agents with better solubility and stability, the variety of target compounds would be significantly expanded (Fig. 18).

We envisage that further developments of the materials chemistry of triplet-DNP provide innovative technologies and new sciences. Low-cost room-temperature triplet-DNP instruments may be installed at local hospitals one day for highly sensitive MRI. The unprecedented polarization enhancement by *in-vivo* triplet-DNP would offer new scientific advancements in the understanding of protein dynamics and metabolic processes. In addition, we see the emergence of a new field of chemistry as a key component in applying quantum physics to biology problems, and we call it as quantum-bio-chemistry.

Conflicts of interest

There are no conflicts to declare.

Acknowledgements

References

1.	A. G. Palmer, J. Williams and A. McDermott, *J. Phys. Chem.*, 1996, **100**, 13293-13310.
2.	C. S. Johnson, *Prog. Nucl. Magn. Reson. Sp.*, 1999, **34**, 203-256.
3.	M. Sattler, *Prog. Nucl. Magn. Reson. Sp.*, 1999, **34**, 93-158.
4.	D. Massiot, F. Fayon, M. Capron, I. King, S. Le Calvé, B. Alonso, J.-O. Durand, B. Bujoli, Z. Gan and G. Hoatson, *Magn. Reson. Chem.*, 2002, **40**, 70-76.
5.	B. Meyer and T. Peters, *Angew. Chem. Int. Ed.*, 2003, **42**, 864-890.
6.	R. Fu, W. W. Brey, K. Shetty, P. Gor'kov, S. Saha, J. R. Long, S. C. Grant, E. Y. Chekmenev, J. Hu, Z. Gan, M. Sharma, F. Zhang, T. M. Logan, R. Bruschweiler, A. Edison, A. Blue, I. R. Dixon, W. D. Markiewicz and T. A. Cross, *J. Magn. Reson.*, 2005, **177**, 1-8.
7.	K. Hashi, S. Ohki, S. Matsumoto, G. Nishijima, A. Goto, K. Deguchi, K. Yamada, T. Noguchi, S. Sakai, M. Takahashi, Y. Yanagisawa, S. Iguchi, T. Yamazaki, H. Maeda, R. Tanaka, T. Nemoto, H. Suematsu, T. Miki, K. Saito and T. Shimizu, *J. Magn. Reson.*, 2015, **256**, 30-33.
8.	G. K. Walters, F. D. Colegrove and L. D. Schearer, *Phys. Rev. Lett.*, 1962, **8**, 439-442.
9.	W. Happer, *Rev. Mod. Phys.*, 1972, **44**, 169-249.
10.	T. G. Walker and W. Happer, *Rev. Mod. Phys.*, 1997, **69**, 629-642.
11.	I. C. Ruset, S. Ketel and F. W. Hersman, *Phys. Rev. Lett.*, 2006, **96**, 4.
12.	C. R. Bowers and D. P. Weitekamp, *J. Am. Chem. Soc.*, 1987, **109**, 5541-5542.
13.	S. Aime, R. Gobetto, F. Reineri and D. Canet, *J. Chem. Phys.*, 2003, **119**, 8890-8896.
14.	T. Jonischkeit, U. Bommerich, J. Stadler, K. Woelk, H. G. Niessen and J. Bargon, *J. Chem. Phys.*, 2006, **124**, 5.
15.	K. V. Kovtunov, V. V. Zhivonitko, A. Corma and I. V. Koptyug, *J. Phys. Chem. Lett.*, 2010, **1**, 1705-1708.
16.	M. Roth, A. Koch, P. Kindervater, J. Bargon, H. W. Spiess and K. Munnemann, *J. Magn. Reson.*, 2010, **204**, 50-55.
17.	R. W. Adams, J. A. Aguilar, K. D. Atkinson, M. J. Cowley, P. I. P. Elliott, S. B. Duckett, G. G. R. Green, I. G. Khazal, J. Lopez-Serrano and D. C. Williamson, *Science*, 2009, **323**, 1708-1711.
18.	T. Theis, M. L. Truong, A. M. Coffey, R. V. Shchepin, K. W. Waddell, F. Shi, B. M. Goodson, W. S. Warren and E. Y. Chekmenev, *J. Am. Chem. Soc.*, 2015, **137**, 1404-1407.
19.	T. Theis, G. X. Ortiz, A. W. J. Logan, K. E. Claytor, Y. Feng, W. P. Huhn, V. Blum, S. J. Malcolmson, E. Y. Chekmenev, Q. Wang and W. S. Warren, *Sci. Adv.*, 2016, **2**, 7.
20.	P. J. Rayner, P. Norcott, K. M. Appleby, W. Iali, R. O. John, S. J. Hart, A. C. Whitwood and S. B. Duckett, *Nat. Commun.*, 2018, **9**.
21.	J. H. Ardenkjaer-Larsen, B. Fridlund, A. Gram, G. Hansson, L. Hansson, M. H. Lerche, R. Servin, M. Thaning and K. Golman, *Proc. Natl. Acad. Sci. U. S. A.*, 2003, **100**, 10158-10163.
22.	C. Song, K.-N. Hu, C.-G. Joo, T. M. Swager and R. G. Griffin, *J. Am. Chem. Soc.*, 2006, **128**, 11385-11390.
23.	V. S. Bajaj, M. L. Mak-Jurkauskas, M. Belenky, J. Herzfeld and R. G. Griffin, *Proc. Natl. Acad. Sci. U. S. A.*, 2009, **106**, 9244-9249.
24.	M. H. Lerche, S. Meier, P. R. Jensen, H. Baumann, B. O. Petersen, M. Karlsson, J. O. Duus and J. H. Ardenkjaer-Larsen, *J. Magn. Reson.*, 2010, **203**, 52-56.
25.	A. J. Rossini, A. Zagdoun, M. Lelli, A. Lesage, C. Coperet and L. Emsley, *Acc. Chem. Res.*, 2013, **46**, 1942-1951.
26.	D. Gajan, A. Bornet, B. Vuichoud, J. Milani, R. Melzi, H. A. van Kalkeren, L. Veyre, C. Thieuleux, M. P. Conley, W. R. Gruening, M. Schwarzwaelder, A. Lesage, C. Coperet, G. Bodenhausen, L. Emsley and S. Jannin, *Proc. Natl. Acad. Sci. U. S. A.*, 2014, **111**, 14693-14697.
27.	A. Fori, M. Liserani, S. Bowen, J. H. Ardenkjaer-Larsen and L. Menichetti, *J. Phys. Chem. A*, 2015, **119**, 1885-1893.
28.	A. Capozzi, T. Cheng, G. Boero, C. Roussel and A. Comment, *Nat. Commun.*, 2017, **8**.
29.	J. N. Dumez, B. Vuichoud, D. Mammoli, A. Bornet, A. C. Pinon, G. Stevanato, B. Meier, G. Bodenhausen, S. Jannin and M. H. Levitt, *J. Phys. Chem. Lett.*, 2017, **8**, 3549-3555.
30.	P. Niedbalski, A. Kiswandhi, C. Parish, Q. Wang, F. Khashami and L. Lumata, *J. Phys. Chem. Lett.*, 2018, **9**, 5481-5489.
31.	J. H. Ardenkjaer-Larsen, S. Bowen, J. R. Petersen, O. Rybalko, M. S. Vinding, M. Ullisch and N. C. Nielsen, *Magn. Reson. Med.*, 2019, **81**, 2184-2194.
32.	S. Jannin, J. N. Dumez, P. Giraudeau and D. Kurzbach, *J. Magn. Reson.*, 2019, **305**, 41-50.
33.	M. S. Albert, G. D. Cates, B. Driehuys, W. Happer, B. Saam, C. S. Springer and A. Wishnia, *Nature*, 1994, **370**, 199-201.
34.	A. M. Oros and N. J. Shah, *Phys. Med. Biol.*, 2004, **49**, 105-153.
35.	M. G. Shapiro, R. M. Ramirez, L. J. Sperling, G. Sun, J. Sun, A. Pines, D. V. Schaffer and V. S. Bajaj, *Nat. Chem.*, 2014, **6**, 630-635.
36.	Y. F. Wang and I. J. Dmochowski, *Acc. Chem. Res.*, 2016, **49**, 2179-2187.
37.	M. Roth, P. Kindervater, H. P. Raich, J. Bargon, H. W. Spiess and K. Munnemann, *Angew. Chem. Int. Ed.*, 2010, **49**, 8358-8362.
38.	S. B. Duckett and R. E. Mewis, *Acc. Chem. Res.*, 2012, **45**, 1247-1257.
39.	J. B. Hovener, A. N. Pravdivtsev, B. Kidd, C. R. Bowers, S. Gloggler, K. V. Kovtunov, M. Plaumann, R. Katz-Brull, K. Buckenmaier, A. Jerschow, F. Reineri, T. Theis, R. V. Shchepin, S. Wagner, P. Bhattacharya, N. M. Zacharias and E. Y. Chekmenev, *Angew. Chem. Int. Ed.*, 2018, **57**, 11140-11162.
40.	P. J. Rayner and S. B. Duckett, *Angew. Chem. Int. Ed.*, 2018, **57**, 6742-6753.

41. R. A. Green, R. W. Adams, S. B. Duckett, R. E. Mewis, D. C. Williamson and G. G. R. Green, *Prog. Nucl. Magn. Reson. Sp.*, 2012, **67**, 1-48.

42. K. R. Keshari and D. M. Wilson, *Chem. Soc. Rev.*, 2014, **43**, 1627-1659.

43. Y. Su, L. Andreas and R. G. Griffin, *Annu. Rev. Biochem.*, 2015, **84**, 465-497.

44. M. E. Halse, *Trac-Trends Anal. Chem.*, 2016, **83**, 76-83.

45. K. V. Kovtunov, E. V. Pokochueva, O. G. Salnikov, S. F. Cousin, D. Kurzbach, B. Vuichoud, S. Jannin, E. Y. Chekmenev, B. M. Goodson, D. A. Barskiy and I. V. Koptyug, *Chem. -Asian J.*, 2018, **13**, 1857-1871.

46. J. H. Ardenkjaer-Larsen, *J. Magn. Reson.*, 2016, **264**, 3-12.

47. S. J. Nelson, J. Kurhanewicz, D. B. Vigneron, P. E. Z. Larson, A. L. Harzstark, M. Ferrone, M. Van Criekinge, J. W. Chang, R. Bok, I. Park, G. Reed, L. Carvajal, E. J. Small, P. Munster, V. K. Weinberg, J. H. Ardenkjaer-Larsen, A. P. Chen, R. E. Hurd, L. I. Odegardstuen, F. J. Robb, J. Tropp and J. A. Murray, *Sci. Transl. Med.*, 2013, **5**, 198ra108-198ra191.

48. A. Flori, M. Liserani, F. Frijia, G. Giovannetti, V. Lionetti, V. Casieri, V. Positano, G. D. Aquaro, F. A. Recchia, M. F. Santarelli, L. Landini, J. H. Ardenkjaer-Larsen and L. Menichetti, *Contrast Media Mol. I.*, 2015, **10**, 194-202.

49. M. Ragavan, L. I. Iconaru, C.-G. Park, R. W. Kriwacki and C. Hilty, *Angew. Chem. Int. Ed.*, 2017, **56**, 7070-7073.

50. I. Park, C. von Morze, J. M. Lupo, J. H. Ardenkjaer-Larsen, A. Kadambi, D. B. Vigneron and S. J. Nelson, *Magn. Reson. Med.*, 2017, **77**, 841-847.

51. C. Kjeldsen, J. H. Ardenkjaer-Larsen and J. O. Duus, *J. Am. Chem. Soc.*, 2018, **140**, 3030-3034.

52. J. R. Brender, S. Kishimoto, H. Merkle, G. Reed, R. E. Hurd, A. P. Chen, J. H. Ardenkjaer-Larsen, J. Munasinghe, K. Saito, T. Seki, N. Oshima, K. Yamamoto, P. L. Choyke, J. Mitchell and M. C. Krishna, *Sci. Rep.*, 2019, **9**, 14.

53. R. D. Bates and W. S. Drozdoski, *J. Chem. Phys.*, 1977, **67**, 4038-4044.

54. B. Borah and R. G. Bryant, *J. Chem. Phys.*, 1981, **75**, 3297-3300.

55. P. Hofer, G. Parigi, C. Luchinat, P. Carl, G. Guthausen, M. Reese, T. Carlomagno, C. Griesinger and M. Bennati, *J. Am. Chem. Soc.*, 2008, **130**, 3254-3255.

56. B. D. Armstrong and S. G. Han, *J. Am. Chem. Soc.*, 2009, **131**, 4641-4647.

57. G. Liu, M. Levien, N. Karschin, G. Parigi, C. Luchinat and M. Bennati, *Nat. Chem.*, 2017, **9**, 676-680.

58. V. Jacques, P. Neumann, J. Beck, M. Markham, D. Twitchen, J. Meijer, F. Kaiser, G. Balasubramanian, F. Jelezko and J. Wrachtrup, *Phys. Rev. Lett.*, 2009, **102**.

59. J. P. King, K. Jeong, C. C. Vassiliou, C. S. Shin, R. H. Page, C. E. Avalos, H.-J. Wang and A. Pines, *Nat. Commun.*, 2015, **6**, 8965.

60. A. Ajoy, K. Liu, R. Nazaryan, X. Lv, P. R. Zangara, B. Safvati, G. Wang, D. Arnold, G. Li, A. Lin, P. Raghavan, E. Druga, S. Dhomkar, D. Pagliero, J. A. Reimer, D. Suter, C. A. Meriles and A. Pines, *Sci. Adv.*, 2018, **4**, eaar5492.

61. A. Henstra, T. S. Lin, J. Schmidt and W. T. Wenckebach, *Chem. Phys. Lett.*, 1990, **165**, 6-10.

62. J.-L. Ong, D. J. Sloop and T.-S. Lin, *Chem. Phys. Lett.*, 1995, **241**, 540-546.

63. M. Iinuma, I. Shake, R. Takizawa, M. Daigo, H. M. Shimizu, Y. Takahashi, A. Masaike and T. Yabuzaki, *Phys. Lett. A*, 1995, **208**, 251-256.

64. M. Iinuma, Y. Takahashi, I. Shake, M. Oda, A. Masaike, T. Yabuzaki and H. M. Shimizu, *Phys. Rev. Lett.*, 2000, **84**, 171-174.

65. K. Takeda, K. Takegoshi and T. Terao, *Chem. Phys. Lett.*, 2001, **345**, 166-170.

66. K. Takeda, K. Takegoshi and T. Terao, *J. Phys. Soc. Jpn.*, 2004, **73**, 2319-2322.

67. K. Takeda, K. Takegoshi and T. Terao, *J. Phys. Soc. Jpn.*, 2004, **73**, 2313-2318.

68. M. Iinuma, Y. Takahashi, I. Shake, M. Oda, H. M. Shimizu, A. Masaike and T. Yabuzaki, *J. Phys. Soc. Jpn.*, 2005, **74**, 2622-2630.

69. M. Iinuma, Y. Takahashi, I. Shake, M. Oda, A. Masaike, T. Yabuzaki and H. M. Shimizu, *J. Magn. Reson.*, 2005, **175**, 235-241.

70. A. Kagawa, Y. Murokawa, K. Takeda and M. Kitagawa, *J. Magn. Reson.*, 2009, **197**, 9-13.

71. A. Kagawa, M. Negoro, K. Takeda and M. Kitagawa, *Rev. Sci. Instrum.*, 2009, **80**, 6.

72. M. Negoro, K. Nakayama, K. Tateishi, A. Kagawa, K. Takeda and M. Kitagawa, *J. Chem. Phys.*, 2010, **133**, 6.

73. T. R. Eichhorn, M. Haag, B. van den Brandt, P. Hautle and W. T. Wenckebach, *Chem. Phys. Lett.*, 2013, **555**, 296-299.

74. T. R. Eichhorn, M. Haag, B. van den Brandt, P. Hautle, W. T. Wenckebach, S. Jannin, J. J. van der Klink and A. Comment, *J. Magn. Reson.*, 2013, **234**, 58-66.

75. K. Tateishi, M. Negoro, A. Kagawa and M. Kitagawa, *Angew. Chem. Int. Ed.*, 2013, **52**, 13307-13310.

76. K. Tateishi, M. Negoro, A. Kagawa, T. Uesaka and M. Kitagawa, *J. Phys. Soc. Jpn.*, 2013, **82**, 5.

77. T. R. Eichhorn, B. van den Brandt, P. Hautle, A. Henstra and W. T. Wenckebach, *Mol. Phys.*, 2014, **112**, 1773-1782.

78. A. Henstra and W. T. Wenckebach, *Mol. Phys.*, 2014, **112**, 1761-1772.

79. K. Tateishi, M. Negoro, S. Nishida, A. Kagawa, Y. Morita and M. Kitagawa, *Proc. Natl. Acad. Sci. U. S. A.*, 2014, **111**, 7527-7530.

80. T. Kawahara, S. Sakaguchi, K. Tateishi, T. L. Tang and T. Uesaka, *J. Phys. Soc. Jpn.*, 2015, **84**, 7.

81. D. J. Sloop, *J. Chem. Phys.*, 1981, **75**, 3746.

82. S. Sakaguchi, Y. Iseri, T. Uesaka, M. Tanifuji, K. Amos, N. Aoi, Y. Hashimoto, E. Hiyama, M. Ichikawa, Y. Ichikawa, S. Ishikawa, K. Itoh, M. Itoh, H. Iwasaki, S. Karataglidis, T. Kawabata, T. Kawahara, H. Kuboki, Y. Maeda, R. Matsuo, T. Nakao, H. Okamura, H. Sakai, Y. Sasamoto, M. Sasano, Y. Satou, K. Sekiguchi, M. Shinohara, K. Suda, D. Suzuki, Y. Takahashi, A. Tamii, T. Wakui, K. Yako, M. Yamaguchi and Y. Yamamoto, *Phys. Rev. C*, 2011, **84**.

83. M. Negoro, K. Tateishi, A. Kagawa and M. Kitagawa, *Phys. Rev. Lett.*, 2011, **107**.

84. M. Haag, B. van den Brandt, T. R. Eichhorn, P. Hautle and W. T. Wenckebach, *Nucl. Instrum. Meth. A*, 2012, **678**, 91-97.

85. T. R. Eichhorn, N. Niketic, B. van den Brandt, U. Filges, T. Panzner, E. Rantsiou, W. T. Wenckebach and P. Hautle, *Nucl. Instrum. Meth. A*, 2014, **754**, 10-14.

86. N. Niketic, B. Van Den Brandt, W. T. Wenckebach, J. Kohlbrecher and P. Hautle, *J. Appl. Crystallogr.*, 2015, **48**, 1514-1521.

87. S. Chebotaryov, S. Sakaguchi, T. Uesaka, T. Akieda, Y. Ando, M. Assie, D. Beaumel, N. Chiga, M. Dozono, A. Galindo-Uribarri, B. Heffron, A. Hirayama, T. Isobe, K. Kaki, S.

Kawase, W. Kim, T. Kobayashi, H. Kon, Y. Kondo, Y. Kubota, S. Leblond, H. Lee, T. Lokotko, Y. Maeda, Y. Matsuda, K. Miki, E. Milman, T. Motobayashi, T. Mukai, S. Nakai, T. Nakamura, A. Ni, T. Noro, S. Ota, H. Otsu, T. Ozaki, V. Panin, S. Park, A. Saito, H. Sakai, M. Sasano, H. Sato, K. Sekiguchi, Y. Shimizu, I. Stefan, L. Stuhl, M. Takaki, K. Taniue, K. Tateishi, S. Terashima, Y. Togano, T. Tomai, Y. Wada, T. Wakasa, T. Wakui, A. Watanabe, H. Yamada, Z. Yang, M. Yasuda, J. Yasuda, K. Yoneda and J. Zenihiro, *Prog. Theor. Exp. Phys.*, 2018, **2018**, 053D001.

88. Y. Quan, B. van den Brandt, J. Kohlbrecher, W. T. Wenckebach and P. Hautle, *Nucl. Instrum. Meth. A*, 2019, **921**, 22-26.

89. G. Maier, U. Haeberlen, H. C. Wolf and K. H. Hausser, *Phys. Lett. A*, 1967, **25**, 384-385.

90. P. Lau, D. Stehlik and K. H. Hausser, *J. Magn. Reson.*, 1974, **15**, 270-282.

91. J. P. Colpa and D. Stehlik, *Chem. Phys.*, 1977, **21**, 273-288.

92. D. Stehlik and J. P. Colpa, *Chem. Phys.*, 1977, **21**, 289-299.

93. D. Stehlik, P. Rosch, P. Lau, H. Zimmermann and K. H. Hausser, *Chem. Phys.*, 1977, **21**, 301-309.

94. J. Allgeier, V. Macho, D. Stehlik, H. M. Vieth, W. Auch and J. U. Vonschutz, *Chem. Phys. Lett.*, 1982, **86**, 522-527.

95. M. Deimling, H. Brunner, K. P. Dinse, K. H. Hausser and J. P. Colpa, *J. Magn. Reson.*, 1980, **39**, 185-202.

96. K. Takeda, *Triplet State Dynamic Nuclear Polarization: Basics, Concepts, Methods*, VDM Publishing, 2009.

97. C. Hintze, U. E. Steiner and M. Drescher, *ChemPhysChem*, 2017, **18**, 6-16.

98. A. J. Van Strien and J. Schmidt, *Chem. Phys. Lett.*, 1980, **70**, 513-517.

99. K. Takeda, *J. Magn. Reson.*, 2008, **192**, 218-229.

100. O. M. Yaghi, M. O'Keeffe, N. W. Ockwig, H. K. Chae, M. Eddaoudi and J. Kim, *Nature*, 2003, **423**, 705-714.

101. S. Kitagawa, R. Kitaura and S. Noro, *Angew. Chem. Int. Ed.*, 2004, **43**, 2334-2375.

102. G. Ferey and C. Serre, *Chem. Soc. Rev.*, 2009, **38**, 1380-1399.

103. Y. Inokuma, M. Kawano and M. Fujita, *Nat. Chem.*, 2011, **3**, 349-358.

104. J.-R. Li, J. Sculley and H.-C. Zhou, *Chem. Rev.*, 2012, **112**, 869-932.

105. K. Sumida, D. L. Rogow, J. A. Mason, T. M. McDonald, E. D. Bloch, Z. R. Herm, T.-H. Bae and J. R. Long, *Chem. Rev.*, 2012, **112**, 724-781.

106. P. Ramaswamy, N. E. Wong and G. K. H. Shimizu, *Chem. Soc. Rev.*, 2014, **43**, 5913-5932.

107. M. C. So, G. P. Wiederrecht, J. E. Mondloch, J. T. Hupp and O. K. Farha, *Chem. Commun.*, 2015, **51**, 3501-3510.

108. L. Sun, M. G. Campbell and M. Dinca, *Angew. Chem. Int. Ed.*, 2016, **55**, 3566-3579.

109. S. Fujiwara, M. Hosoyamada, K. Tateishi, T. Uesaka, K. Ideta, N. Kimizuka and N. Yanai, *J. Am. Chem. Soc.*, 2018, **140**, 15606-15610.

110. K. Nishimura, H. Kouno, K. Tateishi, T. Uesaka, K. Ideta, N. Kimizuka and N. Yanai, *Phys. Chem. Chem. Phys.*, 2019, **21**, 16408-16412.

111. M. Negoro, A. Kagawa, K. Tateishi, Y. Tanaka, T. Yuasa, K. Takahashi and M. Kitagawa, *J. Phys. Chem. A*, 2018, **122**, 4294-4297.

112. A. Kagawa, K. Miyanishi, N. Ichijo, M. Negoro, Y. Nakamura, H. Enozawa, T. Murata, Y. Morita and M. Kitagawa, *J. Magn. Reson.*, 2019, **309**, 5.

113. A. Kagawa, M. Negoro, R. Ohba, N. Ichijo, K. Takamine, Y. Nakamura, T. Murata, Y. Morita and M. Kitagawa, *J. Phys. Chem. A*, 2018, **122**, 9670-9675.

114. S. Astilean, A. Corval, R. Casalegno and H. P. Trommsdorff, *J. Lumin.*, 1994, **62**, 245-252.

115. K. Tateishi, M. Negoro, H. Nonaka, A. Kagawa, S. Sando, S. Wada, M. Kitagawa and T. Uesaka, *Phys. Chem. Chem. Phys.*, 2019, **21**, 19737-19741.

116. H. Kouno, Y. Kawashima, K. Tateishi, T. Uesaka, N. Kimizuka and N. Yanai, *J. Phys. Chem. Lett.*, 2019, **10**, 2208-2213.

117. T. Harris, O. Szekely and L. Frydman, *J. Phys. Chem. B*, 2014, **118**, 3281-3290.

118. D. Kurzbach, E. Canet, A. G. Flamm, A. Jhajharia, E. M. M. Weber, R. Konrat and G. Bodenhausen, *Angew. Chem. Int. Ed.*, 2017, **56**, 389-392.

119. J. Kim, R. Mandal and C. Hilty, *J. Phys. Chem. Lett.*, 2019, **10**, 5463-5467.

120. A. Sadet, C. Stavarache, M. Bacalum, M. Radu, G. Bodenhausen, D. Kurzbach and P. R. Vasos, *J. Am. Chem. Soc.*, 2019, **141**, 12448-12452.

121. H. Kouno, K. Orihashi, K. Nishimura, Y. Kawashima, K. Tateishi, T. Uesaka, N. Kimizuka and N. Yanai, *Chem. Commun.*, DOI: 10.1039/D0CC00836B.

122. K. Ishiba, T. Noguchi, H. Iguchi, M. Morikawa, K. Kaneko and N. Kimizuka, *Angew. Chem. Int. Ed.*, 2017, **56**, 2974-2978.